DE GRUYTER OPEN

Dielectric and Raman studies of $Ba_{0.06}(Na_{1/2}Bi_{1/2})_{0.94}TiO_3–NaNbO_3$ ceramics

SUMIT K. ROY[1], S. CHAUDHURI[1], R.K. KOTNALA[2], D.K. SINGH[2], B.P. SINGH[2], S.N. SINGH[3], K.P. CHANDRA[4], K. PRASAD[5,6,*]

[1]Department of Physics, St. Xavier's College, Ranchi-834 001, India

[2]National Physical Laboratory, New Delhi-110 012, India

[3]University Department of Physics, Ranchi University, Ranchi-834 008, India

[4]Department of Physics, S.M. College, Bhagalpur-812 001, India

[5]Aryabhatta Centre for Nanoscience and Nanotechnology, Aryabhatta Knowledge University, Patna-800 001, India

[6]University Department of Physics, T.M. Bhagalpur University, Bhagalpur 812 007, India

In this work the X-ray diffraction, scanning electron microscopy, Raman and dielectric studies of lead free perovskite $(1−x)Ba_{0.06}(Na_{1/2}Bi_{1/2})_{0.94}TiO_3–xNaNbO_3$ ($0 \leqslant x \leqslant 1.0$) ceramics, prepared using a standard solid state reaction method, were investigated. X-ray diffraction studies of all the ceramics suggested the formation of single phase with crystal structure transforming from rhombohedral-tetragonal to orthorhombic symmetry with the increase in $NaNbO_3$ content. Raman spectra also confirmed the formation of solid solution without any new phase. Dielectric studies showed that the phase transition is of diffusive character and diffusivity parameter decreases with increasing $NaNbO_3$ content. The compositional fluctuation was considered to be the main cause of diffusivity.

Keywords: *lead-free; structure; dielectric constant; Raman spectroscopy*

1. Introduction

Ceramics with perovskite ABO_3-type structures have received considerable attention due to their excellent functional properties and technological relevance. They are widely used in various electronic and microelectronic devices, such as capacitors, piezoelectric transducers, pyroelectric detectors/sensors, memory, electro-optic, magneto-electric devices, SAW substrates, MEMS, etc. [1]. Though the materials used for the fabrication of such devices, mostly lead-based, such as lead titanate, lead magnesium niobate, lead zirconate titanate (PZT), etc. have so long been of paramount importance due to the absence of proper alternatives, there is a global concern nowadays to develop environment-friendly lead-free materials which should have either superior or comparable properties compared to their lead based counterparts [2–8]. One of the major concerns in the replacement of lead ions with non-lead ions retaining essential ferroelectric as well as piezoelectric properties is high polarizability, i.e. a large crystal radius, high effective number of electrons and presence of lone pair electrons in the outer shell. Fortunately, bismuth (Bi) has high polarizability (>5 Å^3) [9]. Also, it is non-toxic and has no harmful effect on environment. Hence, Bi-based compounds seem to be the most likely replacement to the lead-based materials [6, 10]. It is observed that among the Bi-based systems, $(1−x)(Bi_{1/2}Na_{1/2})TiO_3–xBaTiO_3$ is considered to be one of the potential lead-free candidates for dielectric and/or piezoelectric applications. It exhibits a rhombohedral-tetragonal morphotropic phase boundary (MPB) around $0.06 \leqslant x \leqslant 0.08$ with remarkable piezoelectric and electro-magnetic properties [11–14]. Besides, sodium

*E-mail: k.prasad65@gmail.com

niobate ($NaNbO_3$) is a dielectric material having a perovskite-type structure, exhibiting large number of successive phase transitions and is one of the most complex perovskite ferroelectric materials [15–17]. At room temperature it shows antiferroelectric behavior, with a Curie temperature of 360 °C [18, 19].

Recently, the dielectric and relaxor behavior of $BaTiO_3$–$NaNbO_3$ [20], $A_{0.5}Bi_{0.5}TiO_3$–$NaNbO_3$ (A = Li, Na, K, Ag) [21], $BaSnO_3$–$NaNO_3$ [22], $Sr_{0.5}NbO_3$–$LiNbO_3$–$NaNbO_3$ [23], $(Bi_{0.5}Na_{0.5})_{0.94}Ba_{0.06}(Ti_{1-5x/4}Nb_x)O_3$ [24] and $(Bi_{0.5}Na_{0.5})_{0.935}Ba_{0.065}Ti_{(1-x)}Nb_xO_3$–$0.01SrZrO_3$ [25] ceramic solid solutions have been studied. Xu et al. [26] have studied the phase transitions, formation enthalpies and implications for general perovskite energetics with special reference to $SrTiO_3$–$NaNbO_3$ solid solution, while magnetic and ferroelectric phase transitions studies in $BiFeO_3$–$NaNbO_3$ system were carried out by Raevski et al. [27]. Besides, microstructural, Raman and dielectric properties of $(1-x)NaNbO_3$–$xBiCrO_3$ biphase ceramic system have been studied by Hsiao et al. [28]. Furthermore, the electrical properties of a number of solid-solutions of $BaTiO_3$ [29, 30], $(A_{0.5}Bi_{0.5})TiO_3$ (A = Na, K) [31, 32], $SrTiO_3$ [33], $AgNbO_3$–$KNbO_3$ [34], $Bi(Zn_{0.5}Ti_{0.5})O_3$ [35], $BaTiO_3$–$Bi(Zn_{1/2}Ti_{1/2})O_3$ [36], $Ba_{0.8}Ca_{0.2}TiO_3$–$Bi(Mg_{0.5}Ti_{0.5})O_3$ [37], $CaZrO_3$ [38], with $NaNbO_3$ have been reported recently. However, no report to the best of authors' knowledge, has so far been presented on the non-lead pseudo-binary $Ba_{0.06}(Na_{1/2}Bi_{1/2})_{0.94}TiO_3$–$NaNbO_3$ solid-solution system and this fact motivates this research. Both $Ba_{0.06}(Na_{1/2}Bi_{1/2})_{0.94}TiO_3$ and $NaNbO_3$ are typical perovskite-type compounds and could be expected to form a solid solution. The elements present at A-site in $Ba_{0.06}(Bi_{1/2}Na_{1/2})_{0.94}TiO_3$ have ionic radii $r(Ba_{XII}^{+2}) = 1.61$ Å, $r(Na_{XII}^{+2}) = 1.03$ Å and $r(Bi_{VIII}^{+3}) = 1.39$ Å. So, the average ionic radius of A-site is $\langle r_A \rangle = 1.234$ Å. Also, the ionic radius of B-site is $\langle r_B \rangle = r(Ti_{VI}^{+4}) = 0.605$ Å. Transition metal Nb in $NaNbO_3$ has the ionic radius $r(Nb_{VI}^{+5}) = 0.69$ Å. Hence, the involved degree

of ionic radius mismatch for the substitution of Nb at A- or B-site is $\Delta r_A = |\langle r_A \rangle - r(Nb_{VI}^{+5})| = 0.544$ Å and $\Delta r_B = |\langle r_B \rangle - r(Nb_{VI}^{+5})| = 0.095$ Å. Thus, Nb_{VI}^{+5} is more likely to be incorporated into the B-site of the BNBT matrix. Inclusion of Nb into B-site also ensures less stress in the lattice as compared to that into A-site. Furthermore, to understand the structure of a material and comparison of similar ions on the same site, Goldschmidt tolerance factor is considered to be a useful tool in determining the correct trends, when used with proper coordination numbers. Considering the tolerance factor, the coulombic and strain interactions and the charge balance, the possible B-site substitution material for the solid solution of $Ba_{0.06}(Na_{1/2}Bi_{1/2})_{0.94}TiO_3$ and $NaNbO_3$ is formulated as $Ba_{0.06(1-x)}Na_{(0.47+0.53x)}Bi_{0.47(1-x)}Ti_{1-x}Nb_xO_3$. Therefore, it is of interest to study the structural and electrical properties of such $Ba_{0.06}(Na_{1/2}Bi_{1/2})_{0.94}TiO_3$–$NaNbO_3$ ceramic system. Accordingly, in the present work, structural (X-ray), microstructural (SEM and EDS), optical (Raman and IR spectroscopy) and dielectric studies of $(1-x)Ba_{0.06}(Na_{1/2}Bi_{1/2})_{0.94}TiO_3$–$xNaNbO_3$ (abbreviated hereafter as BNBT-NN) ceramic system with different compositions ($0 \leqslant x \leqslant 1.0$) have been carried out.

2. Experimental

$Ba_{0.06}(Na_{1/2}Bi_{1/2})_{0.94}TiO_3$ (BNBT) and $NaNbO_3$ (NN) powders were synthesized by using the solid state reaction method. Reagent grade (>99.9 % purity) $BaCO_3$, Na_2CO_3, Bi_2O_3, TiO_2 and Nb_2O_5 were used as starting materials. The starting materials were prepared after removing absorbed water completely at 200 °C for one hour. The mixed powders were calcined at 1140 °C and 850 °C respectively for 5 h in air. Completion of reaction and the formation of desired compounds were checked by X-ray diffraction (XRD) technique. In the present study, the solid solutions of BNBT and NN with different compositions (x = 0.05, 0.10, 0.25, 0.50, 0.75, 0.90 and 0.95) were prepared and were compacted into thin (~1.5 mm) cylindrical disks with an applied

uniaxial pressure of 5000 kg. The samples were finally sintered between 1180 °C and 870 °C for 4 h. The sintered pellets were polished carefully to ensure the parallel and flat surfaces.

The XRD data were obtained on sintered pellets of BNBT-NN with an X-ray diffractometer (X'Pert PRO, PANalytical) at room temperature, using CuKα radiation (λ = 1.5405 Å), over a range of Bragg angles ($10° \leqslant 2\theta \leqslant 70°$) with a scanning speed of 5.08° min^{-1}. The dimensions of the unit cell, h k l values and space group of all the specimens, were obtained using the software X'Pert Highscore Plus. The Raman spectra were obtained using a single monochromator micro-Raman spectrometer (Renishaw inVia Raman Microscope) and excitation wavelengths were provided by a diode laser with an exciting wavelength of 785 nm. The dielectric constants and dielectric loss were measured between 500 °C and 40 °C with a cooling rate of 10 °C/min using a computer-controlled Alpha high resolution dielectric analyzer (NOVO-CONTROL Technologies, GmbH & Co. KG, Germany) on a symmetrical cell of Ag|Ceramic|Ag type, where Ag is an air drying silver conductive paint (SPI, Structure probe, Inc.) coated on either side of the pellets.

3. Results and discussion

3.1. Structural and microstructural studies

Fig. 1a shows the XRD patterns of BNBT-NN samples sintered under air atmosphere. All samples have a perovskite-type structure with different crystal symmetry, and no other peaks were detected within the uncertainty limits of XRD, which suggests the absence of impurity phases. The crystal data of NaNbO$_3$ (x = 1) and BNBT (x = 0), obtained from the XRD analyses, depicted in Table 1, are consistent with the earlier reports [12, 39–41]. Further, a pure perovskite phase with rhombohedral-tetragonal symmetry is found up to the x = 0.25, while the orthorhombic phase starts appearing and becomes noticeable at x = 0.50. The composition with x = 0.50 is found to have a mixed phase

of rhombohedral-tetragonal-orthorhombic symmetry (Table 1). Fig. 1b illustrates the enlarged XRD patterns ($46° \leqslant 2\theta \leqslant 48°$) of all the solid solutions. It can clearly be seen that the crystal structure of the samples at room temperature gradually changes from rhombohedral-tetragonal to orthorhombic symmetry with increasing x, which is apparent by the splitting of 200 reflections into 002 and 200 doublet of orthorhombic phase. The difference in intensity of the splitted peaks becomes prominent from x = 0.75. At very high doping percentages (90 % and 95 %) of NaNbO$_3$, the ceramics shows pure perovskite phase with orthorhombic symmetry. This indicates that NaNbO$_3$ has completely integrated into the lattice of Ba$_{0.06}$(Na$_{1/2}$Bi$_{1/2}$)$_{0.94}$TiO$_3$ and formed the solid solution. Thus, BNBT-NN ceramics shows a coexistence of rhombhohedral-tetragonal-orthorhombic phases at x = 0.50. Furthermore, it is observed that the increment of Nb-content in the solid solution, in general, leads to the increase in unit cell volume which may be attributed to the fact that ionic radius of Nb^{+5} (0.69 Å) ions is slightly larger than that of Ti^{+4} (0.605 Å) ions.

Fig. 2 shows the SEM micrographs of fractured surface of sintered BNBT-NN ceramics. The nature of the micrographs exhibits the polycrystalline texture of the materials, and grains are distributed throughout the samples. The photographs contain a very few voids suggesting the high density of the materials. The grains of unequal sizes (0.8 μm to 3 μm) were found for the chosen compositions. It is also observed that a few grains are agglomerated and appear larger in size compared to the average size, which is termed as an abnormal grain growth or secondary crystallization. The average grain size for BNBT sample is found to be ~3 μm and with increasing NN concentration (x), the grain size as well as grain morphology of BNBT-NN ceramics changes. For x = 0.05 the average grain size significantly decreases to nearly 1.25 μm and some pores begin to appear. Further doping of NN inhibits the grain growth and leads to a decrease in grain size. As the substitution level of NN increases from x = 0.50 to x = 0.75 the grains become further smaller (1 μm to 0.8 μm).

The average grain size of the ceramics becomes minimum when x = 0.75 and increases with further doping. With further increase in NN concentration the average grain size increases slightly to 1 μm. The partial substitution of Ti-ion by Nb-ion results from the differences in their ionic radii, valency and electronegativity which worsen the diffusion coefficient of B-site ion in perovskite lattice [42] and consequently, the grain growth is inhibited with the increase in Nb concentration that results in a decrease in average grain size.

3.2. Raman study

The first-order Raman spectra of the end members $Ba_{0.06}(Na_{1/2}Bi_{1/2})_{0.94}TiO_3$ and $NaNbO_3$ of BNBT-NN ceramics are shown in Fig. 3a and Fig. 3b, respectively. The peaks of BNBT were found to be Gaussian in line-shape contrary to the expected Lorentzian line-shape fitting over the exponential background from Rayleigh tail. The peaks (FWHM in parenthesis) were observed at 133.3 (19.2) cm^{-1}, 281.3 (53.4) cm^{-1}, 536.2 (49.7) cm^{-1}, 615.3 (28.11) cm^{-1} and 799.4 (79.2) cm^{-1}. The Gaussian peak profile observed in the Raman spectra may arise due to the distribution of particle sizes in the sample. Contrary to the BNBT pellets, NN shows intense sharp and multiple Lorentzian peaks (Fig. 3b). It agrees well with the results presented in the literature [29]. A peak at 434.2 cm^{-1} starts appearing from x = 0.5 onwards (Fig. 3c), indicating the change in crystal structure. However, with increasing NN concentration (x), no new peaks are observed, indicating the absence of formation of any new phase and consequently the formation of solid solutions. It can also be seen from Fig. 3c that the bands with lower intensities appear at frequencies that do not differ much from those of the pure NN. Since the Raman spectra of BNBT and NN differ appreciably, the evolution of the structural changes of BNBT-NN solid solutions, which depend on composition, can be followed using XRD and dielectric measurement data. Also, the Raman bands are quite broad, which in fact is associated with the disorder of cations at the coordinated sites, and to some overlapping Raman modes [29].
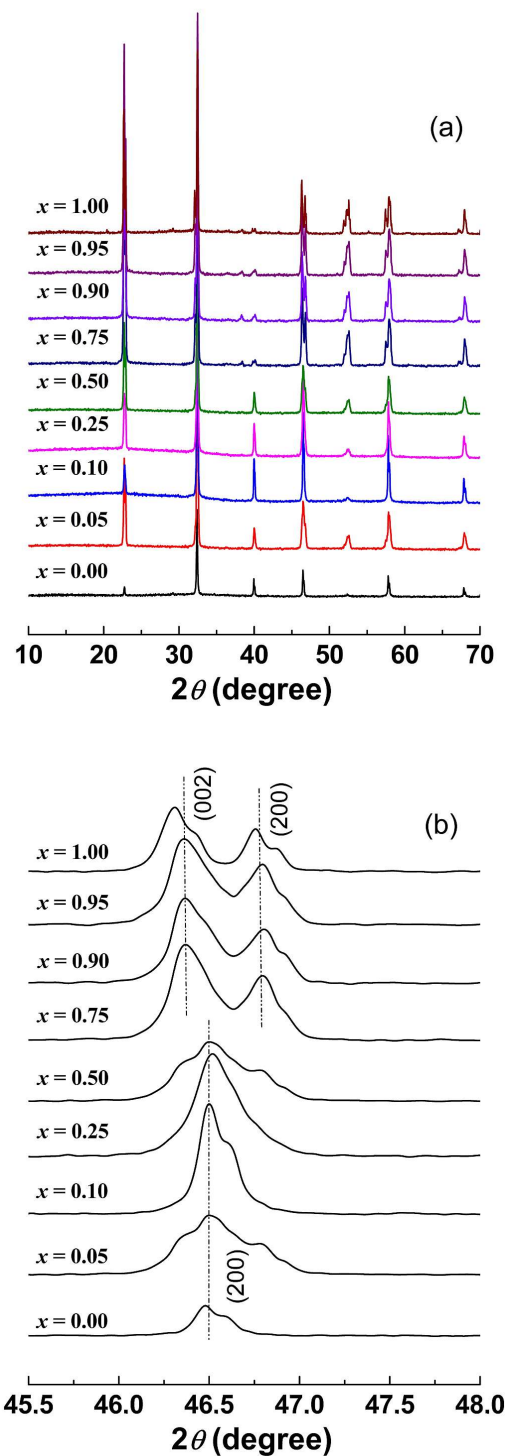

Fig. 1. (a) XRD patterns of $(1-x)Ba_{0.06}(Na_{1/2}Bi_{1/2})_{0.94}$ TiO_3–$xNaNbO_3$ ceramics at room temperature and (b) XRD patterns of $(1-x)Ba_{0.06}(Na_{1/2}Bi_{1/2})_{0.94}TiO_3$–$xNaNbO_3$ ceramics in the selected regions of 2θ (45.5° to 48°).

Table 1. Lattice parameters of the (1 − x)Ba$_{0.06}$(Na$_{1/2}$Bi$_{1/2}$)$_{0.94}$TiO$_3$–xNaNbO$_3$ (0 ⩽ x ⩽ 1) ceramics.

Parameters / x	0.00	0.05	0.10	0.25	0.50	0.75	0.90	0.95	1.00
a [Å]	3.9037	3.8979	3.9033	3.9	3.898	3.935	3.909	3.933	3.95
b [Å]	3.9037	3.8979	3.9033	3.9	3.898	3.912	3.87	3.912	3.84
c [Å]	3.898	3.903	3.909	3.9038	3.907	3.88	3.885	3.88	3.909
c/a	0.998	1.0013	1.0014	1.0009	1.0023	0.9860	0.9938	0.9865	0.9896
Cell volume [Å^3]	58.86	59.29	59.56	59.38	59.36	59.7	58.74	59.7	59.34
Crystal system	R / T	R / T	R / T	R / T	R / T / O	O	O	O	O

Note: T – Tetragonal; O – Orthorhombic and R – Rhombohedral
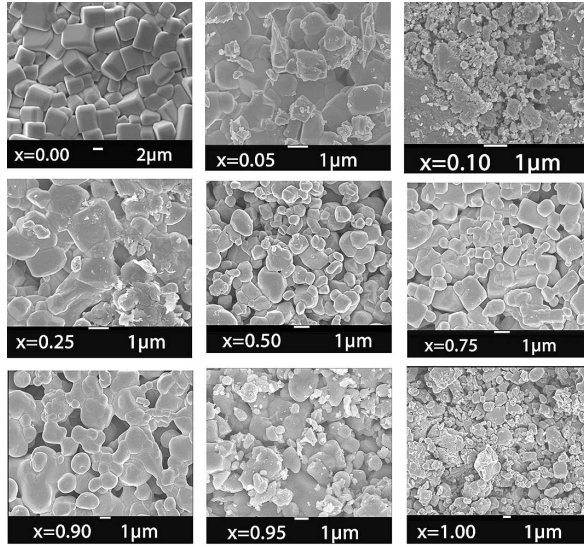
Fig. 2. SEM images of (1 − x)Ba$_{0.06}$(Na$_{1/2}$Bi$_{1/2}$)$_{0.94}$ TiO$_3$–xNaNbO$_3$ ceramics.

Fig. 3. Raman spectra of (a) Ba$_{0.06}$(Na$_{1/2}$Bi$_{1/2}$)$_{0.94}$ TiO$_3$ and peaks fitted with Gaussian components, (b) Raman spectra of NaNbO$_3$ can be deconvoluted with Lorentzian components contrary to Ba$_{0.06}$(Na$_{1/2}$Bi$_{1/2}$)$_{0.94}$TiO$_3$, NaNbO$_3$ requires multiple peaks and (c) shows a change in the Raman spectra with increasing NaNbO$_3$ doping % in Ba$_{0.06}$(Na$_{1/2}$Bi$_{1/2}$)$_{0.94}$TiO$_3$ matrix.

3.3. Dielectric study

Fig. 4 shows the variation of ε with frequency at room temperature. The value of ε is found to decrease with an increase in frequency and beyond 10 kHz it seems to be almost independent of frequency. Also, the value of ε, in general, decreases with the increasing NN-concentration (x).

It is known that the phase transition in ferroelectric ceramics depends mainly on chemical composition, microstructure and sintering processes (preparation condition). The transition region extends over some tens of degrees around the temperature of maximum ε (ε$_{max}$). The electrical polarization, P$_r$, continuously decreases with increasing tempera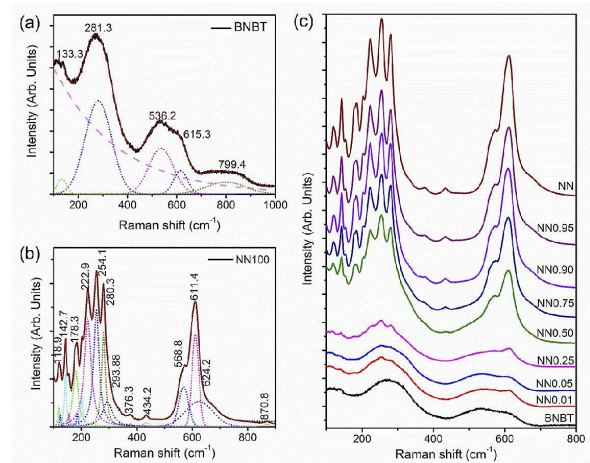ture rendering it difficult to determine the exact temperature when P$_r$ = 0. The anomalies which take place at ferro-paraelectric phase transition in classical perovskite type ferroelectrics are generally described by the susceptibility (χ) and the order parameter (P) by the expression:

$$\chi_{ij}^{-1} = \chi_o^{-1} + \sum g_{ijkl} P_k P_l \qquad (1)$$

The coupling constant g$_{ijkl}$ describes the breaking of symmetry by the phase transition. However, it is seen that there exist a set of anomalies in the behavior of some perovskite ferroelectrics with a diffuse phase transition (DPT) which are difficult to explain on the basis of classical theories
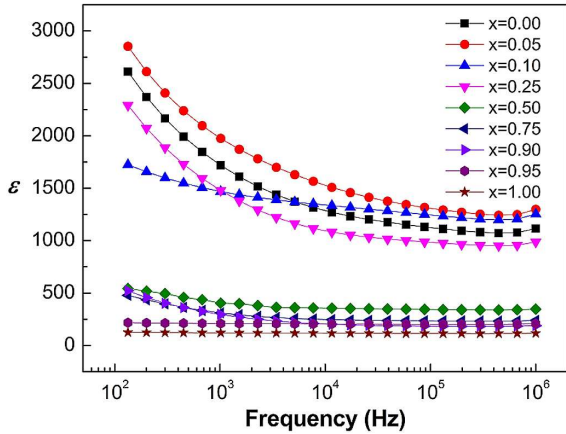
Fig. 4. Frequency dependence of dielectric constant of $(1-x)\mathrm{Ba}_{0.06}(\mathrm{Na}_{1/2}\mathrm{Bi}_{1/2})_{0.94}\mathrm{TiO}_3$–$x\mathrm{NaNbO}_3$ ceramics at room temperature.

of ferroelectrics. The maxima of the dielectric constant in DPTs are not well defined. It is thus experimentally difficult to accurately estimate the temperature of the ferro-paraelectric phase transition, T_m (ε_{max}). In the paraelectric region the dielectric constant exhibits temperature dependence according to the modified Curie-Weiss law:

$$\varepsilon^{-1} = \varepsilon_{max}^{-1} + C'(T - T_m)^\gamma \qquad (2)$$

where ε_{max} is the maximum value of the dielectric constant at T_m, C' and γ (diffusivity parameter) are assumed to be constant, with γ value between 1 and 2. The limiting values $\gamma = 1$ and $\gamma = 2$ are characteristic of a normal ferroelectric and an ideal relaxor ferroelectric, respectively. Fig. 5 shows the variation of dielectric constant (ε) and loss tangent (tanδ) with the increment in temperature at different frequencies for different compositions of BNBT-NN ceramics. As typical of normal ferroelectrics, ε increases gradually with increment in temperature up to the transition temperature (T_m) and then decreases. Also, it is seen that with the increment of NN concentration, maximum value of ε (ε_{max}) decreases while dielectric peak (T_m) shifts towards lower temperature side up to $x = 0.25$ and then it starts shifting towards higher temperature side and $\varepsilon(T)$ curve becomes less diffuse. This result is consistent with the XRD and Raman data as the orthorhombic phase (Table 1)

is coming into force. The decrease in ε_{max} implies that the substitution of NN reduces the dipole moment of the lattice and lowers the peak dielectric constant. In all the materials, the room temperature value of tanδ was found to be of the order of 10^{-2} at 1 kHz. The low tanδ of this kind can be advantageous when improved detectivity is required. Besides, linear fitting of $\varepsilon(T)$ data, in paraelectric phase, in the expression $\varepsilon = C(T - T_o)^{-1}$ allows us to obtain the Curie-Weiss temperature (T_o) for different ceramic compositions: here C is Curie-Weiss constant. It was observed that the value of T_o first shifts towards lower temperature side up to $x = 0.25$ and then it starts shifting towards higher temperature side with the increase in modifier (NN) percentages and $T_o < T_m$ for all materials, which implies that the phase transitions are of the first order.

The regions around the dielectric peaks are broadened (Fig. 5), which is one of the most important characteristics of a disordered perovskite type structure with diffuse phase transition (DPT). Fig. 6 shows the variation of $\ln(1/\varepsilon - 1/\varepsilon_{max})$ with $\ln(T - T_m)$ for three samples ($x = 0$, 0.50 and 1.0) at 1 kHz. The graphs show almost linear behavior as temperature changes. The value of exponent, γ, in expression 2 was estimated, respectively to be 1.92, 1.20 and 1.14 for $x = 0$, 0.50 and 1.0 from the slope of the curves in Fig. 6. We have found $\gamma > 1$ for all the cases, the value of which decreases with an increase in NN content. In other words diffusivity decreases with an increase in NN content. This may be due to compositional fluctuations which might produce some kind of heterogeneities in the arrangement of Ba^{2+} and $(\mathrm{Na}_{0.5}^{1+}\mathrm{Bi}_{0.5}^{3+})^{2+}$ ions at A-site Ti^{4+} and Nb^{5+} ions at B-site that results in decreasing disorder with increasing NN content. This may be explained on the basis of increasing tolerance factor and average ionic radius of A- and B-site cations (Table 2) which results in decreasing disorder as well as dielectric constant as x increases.

4. Conclusion

Lead-free ceramics, $(1-x)\mathrm{Ba}_{0.06}(\mathrm{Na}_{1/2}\mathrm{Bi}_{1/2})_{0.94}\mathrm{TiO}_3$–$x\mathrm{NaNbO}_3$ ($0 \leqslant x \leqslant 1.0$) were
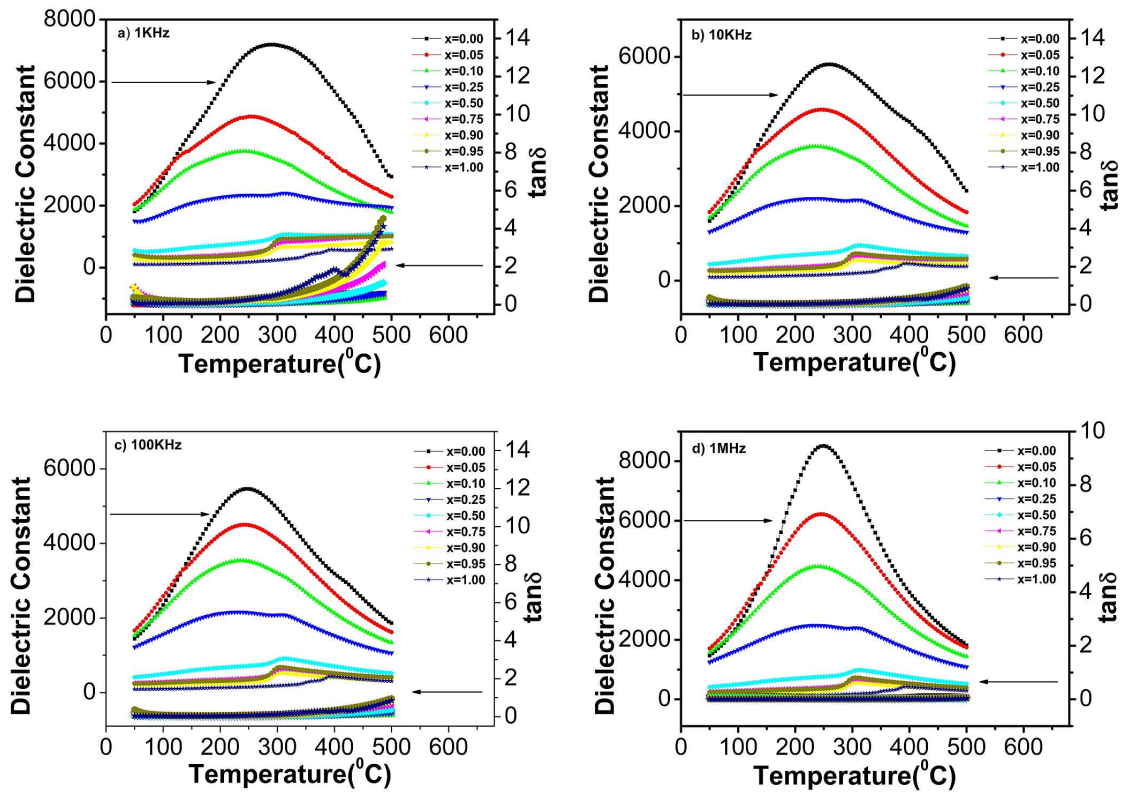
Fig. 5. Temperature dependence of dielectric constant and loss tangent of $(1 - x)$Ba$_{0.06}$(Na$_{1/2}$Bi$_{1/2}$)$_{0.94}$TiO$_3$–xNaNbO$_3$ ceramics at different frequencies (a) 1 kHz (b) 10 kHz (c) 100 kHz (d) 1MHz.

Table 2. Tolerance factor, average A- and B-site ionic radius of $(1-x)$Ba$_{0.06}$(Na$_{1/2}$Bi$_{1/2}$)$_{0.94}$TiO$_3$–xNaNbO$_3$ ceramics.

x	Tolerance factor (t)	Average ionic radius of A site [Å]	Average ionic radius of B site [Å]
0.00	0.950	1.300	0.605
0.05	0.951	1.304	0.607
0.10	0.952	1.309	0.609
0.25	0.955	1.322	0.614
0.50	0.960	1.345	0.623
0.75	0.965	1.367	0.631
0.90	0.968	1.381	0.637
0.95	0.969	1.385	0.638
1.00	0.970	1.390	0.640

synthesized using the solid state reaction method. X-ray diffraction studies of all the ceramics suggested the formation of a single phase with crystal structure transforming from rhombohedral-tetragonal to orthorhombic symmetry with the increase in NaNbO$_3$ content. Raman spectra also confirmed the formation of solid solution without any new phase. The dielectric constant as a function of temperature did not show a sharp transition but exhibited diffuse behavior and the degree of diffuseness decreased from 1.92 to 1.14 with increasing NaNbO$_3$ content from x = 0.0 to 1.0.
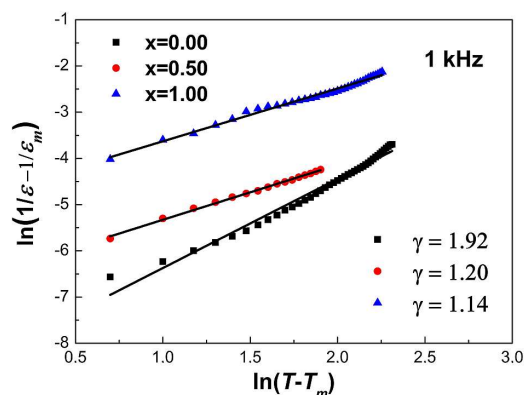
Fig. 6. The modified Curie-Weiss plots $\ln(1/\varepsilon-1/\varepsilon_m)$ vs. $\ln(T-T_m)$ for $(1-x)Ba_{0.06}(Na_{1/2}Bi_{1/2})_{0.94}$ $TiO_3-xNaNbO_3$ ceramics for x = 0, x = 0.50, x = 1.0 at 1 kHz.

The compositional fluctuation was considered to be the main cause for diffusivity.

References

[1] CROSS L.E., *Nature*, 432 (2004), 24.
[2] SEO I.-T., CHOI C.-H., SONG D., JANG M.-S., KIM B.-Y., NAHM S., KIM Y.-S., SUNG T.-H., SONG H.-C., *J. Am. Ceram. Soc.*, 96 (2013), 1024.
[3] DAMJANOVIC D., KLEIN N., LI J., POROKHONSKYY V., *Funct. Mater. Lett.*, 3 (2010), 5.
[4] EICHEL R.-A., KUNGL H., *Funct. Mater. Lett.*, 3 (2010), 1.
[5] PANDA P.K., *J. Mater. Sci.*, 44 (2009), 5049.
[6] RÖDEL J., JO W., SEIFERT K.T.P., ANTON E.-M., GRANZOW T., DAMJANOVIC D., *J. Am. Ceram. Soc.*, 92 (2009), 1153.
[7] SHROUT T.R., ZHANG S.J., *J. Electroceram.*, 19 (2007), 111.
[8] TAKENAKA T., NAGATA H., *J. Eur. Ceram. Soc.*, 25 (2005), 2693.
[9] GRIMES N.W., GRIMES R.W., *J. Phys.-Condens. Mat.*, 10 (1998), 3029.
[10] CHU B.-J., CHEN D.-R., LI G.-R., YIN Q.-R., *J. Eur. Ceram. Soc.*, 22 (2002), 2115.
[11] TAKENAKA T., MARUYAMA K., SAKATA K., *Jpn. J. Appl. Phys.*, 30 (9B) (1991), 2236.
[12] TAKENAKA T., NAGATA H., *J. Eur. Ceram. Soc.*, 25 (2005), 2693.
[13] ROY A.K., SINGH A., KUMARI K., AMARNATH K., PRASAD A., PRASAD K., *ISRN Ceram.*, 2012 (2012), 854831.
[14] ROY A.K., SINGH A., KUMARI K., PRASAD A., PRASAD K., *Phys. Express*, 3 (2013), 14.
[15] LANFREDI S., LENTE M.H., EIRAS J.A., *Appl. Phys. Lett.* 80 (2002), 2731.
[16] HUNGRÍA T., PARDO L., MOURE A., CASTRO A., *J. Alloy. Compd.*, 395 (2005), 166.
[17] ROY S.K., SINGH S.N., KUMAR K., PRASAD K., *Adv. Mater. Res.*, 2 (2013), 173.
[18] KORUZA J., TELLIER J., MALIČ B., BOBNAR V., KOSEC M., *J. Appl. Phys.*, 108 (2010), 113509.
[19] SHANON R.D., *Acta Crystallogr. A*, 32 (1976), 751.
[20] KHEMAKHEM H., SIMON A., MÜHLL R.V.D., RAVEZ J., *J. Phys.-Condens. Mat.*, 12 (2000), 5951.
[21] RAEVSKI I.P., REZNITCHENKO L.A., MALITSKAYA M.A., SHILKINA L.A., LISITSINA S.O., RAEVSKAYA S.I., KUZNETSOVA E.M., *Ferroelectrics*, 299 (2004), 95.
[22] AYDI A., KHEMAKHEM H., BOUDAYA C., VON DER MÜHLL R., SIMON A., *Solid State Sci.*, 6 (2004), 333.
[23] RAEVSKAYA S.I., DELLIS J.L., REZNICHENKO L.A., PROSANDEEV S.A., RAEVSKI I.P., LISITSINAN S.O., JASTRABIK L., *Ferroelectrics*, 317 (2005), 241.
[24] ZEREFFA E.A., PRASADA RAO A.V., *Ceram.-Silikaty*, 58 (2014), 28.
[25] MAQBOOL A., HUSSAIN A., MALIK R.A., ZAMAN A., SONG T.K., KIM W.-J., KIM M.-H., *Korean J. Mater. Res.*, 25 (2015), 317.
[26] XU H., NAVROTSKY A., SU Y., BALMER M.L., *Chem. Mater.*, 17 (2005), 1880.
[27] RAEVSKI I.P., KUBRIN S.P., DELLIS J.-L., RAEVSKAYA S.I., SARYCHEV D.A., SMOTRAKOV V.G., EREMKIN V.V., SEREDKINA M.A., *Ferroelectrics*, 371 (2008), 113.
[28] HSIAO Y.-J., CHANG Y.-H., FANG T-H., CHANG Y-S., CHAI Y.-L., *J. Alloy. Compd.*, 430 (2007), 313.
[29] BAHRI F., KHEMAKHEM H., GARGOURI M., SIMON A., MÜHLL VON DER R., RAVEZ J., *Solid State Sci.*, 5 (2003), 1229.
[30] ABDELKEFI H., KHEMAKHEM H., VELU G., CARRU J.C., MÜHLL VON DER R., *Solid State Sci.*, 6 (2004), 1347.
[31] WADA T., TOYOIKE K., IMANAKA Y., MATSUO Y., *Jpn. J. Appl. Phys.*, 40 (2001), 5703.
[32] LI Y., CHEN W., ZHOU J., XU Q., SUN H., XU R., *Mater. Sci. Eng. B-Adv.*, 112 (2004), 5.
[33] HUNGRÍA T., ALGUER M., CASTRO A., *J. Am. Ceram. Soc.*, 90 (2007), 2122.
[34] CHO J.-H., CHUN M.-P., NAM J.-H., HAN K.-S., KIM B.-I., *J. Korean Phys. Soc.*, 57 (2010), 859.
[35] PRASERTPALICHAT S., CANN D.P., *J. Electroceram.*, 33 (2014), 214.
[36] RAENGTHON N., BROWN-SHAKLEE H.J., BRENNECKA G.L., CANN D.P., *J. Mater. Sci.*, 48 (2013), 2245.
[37] ZEB A., MILNE S.J., *J. Am. Ceram. Soc.*, 96 (2013), 3701.
[38] SHIMIZU H., GUO H., REYES-LILLO S.E., MIZUNO Y., RABE K.M., RANDALL C.A., *Dalton T.*, 44 (2015), 10763.
[39] SIVASUBRAMANIAN V., MURTHY V.R.K., VISWANATHAN B., *Jpn. J. Appl. Phys.*, 36 (1997), 194.
[40] CALDERON-MORENO J.M., CAMARGO E.R., *Catal. Today*, 78 (2003), 539.

[41] KORUZA J., MALIC B., NOSHCHENKO O., KOSEC M., *J. Nanomater.*, 2012 (2012), 469143.

[42] XU C., LIN D., KWOK K.W., *Solid State Sci.*, 10 (2008), 934.